PCCP

Accepted Manuscript

ROYAL SOCIETY OF CHEMISTRY

www.rsc.org/pccp

Physical Chemistry Chemical Physics
CREATED USING THE RSC LaTeX PCCP ARTICLE TEMPLATE – SEE www.rsc.org/electronicfiles FOR DETAILS
ARTICLE TYPE www. rsc.org/xxxxxx | XXXXXXXX

Visible-ultraviolet vibronic emission of silica nanoparticles

Luisa Spallino,[a] Lavinia Vaccaro,[a] Luisa Sciortino,[a] Simonpietro Agnello,[a] Gianpiero Buscarino,[a] Marco Cannas,*[a] and Franco Mario Gelardi[a]

Received Xth XXXXXXXXXX 20XX, Accepted Xth XXXXXXXXX 20XX
First published on the web Xth XXXXXXXXXX 200X
DOI: 10.1039/b000000x

We report the study of the visible-ultraviolet emission properties and the structural features of silica nanoparticles prepared through a laboratory sol-gel technique. Atomic force microscopy, Raman and Infrared investigations highlighted the 10 nm size, purity and porosity of the obtained nanoparticles. By time resolved photoluminescence technique in air and in vacuum we were able to single out two contributions in the visible emission: one, stable in both atmospheres, is a typical fast blue band centered around 2.8 eV; the second, only observed in vacuum around the 3.0-3.5 eV range, is a vibrational progression with two phonon modes at 1370 cm^{-1} and 360 cm^{-1}. By fully characterizing the spectroscopic features of this structured emission, we evidence its vibronic properties and clarify the different origin with respect to the blue luminescent defect.

1 Introduction

Luminescence is a paramount property for several optical applications in the modern nanotechnologies (bioimaging, optoelectronics, photovoltaics)[1–6]. The research is therefore active towards the development of production methods successful to finely control the physical and chemical characteristics of nanostructured materials thus tailoring their emission. Silica nanoparticles (NPs) are systems of choice for this purpose: they combine high luminescence with facile synthesis methods, non toxicity and resistance to thermal and irradiation treatments[7–12]. Their emissivity, surprising if compared to the optical properties of the bulk counterpart, is mainly related to the high specific surface ($\sim 10^2\ m^2\ g^{-1}$) that favors the formation of a wide variety of luminescent defects. The microscopic structure of these sites is also influenced by the surface accessibility to atomic and molecular species of the environment atmosphere[13].

Silica surface is generally terminated with Si-H or Si-OH functional groups, well identified by their IR bands[14]. Some authors suggested that these groups are responsible for the photoluminescence (PL) activity under UV light excitation: Si-H is responsible for a band centered around 2.4 eV with a vibronic progression spacing $\sim$630 cm^{-1} [15], whereas Si-OH gives rise to a PL centered around 3.7 eV[16]. Also molecular oxygen plays a crucial role since it is active in several reactions and it can diffuse through the silica NPs[17,18]. Previous experiments, dealing with the effects induced by controlled thermochemical reactions, have demonstrated the formation of oxygen related defects peculiar to surface such as the nonbridging oxygen, Si-O•, the dioxasilyrane, $Si(O_2)$, and the silanone, Si=O[13,19,20]. The optical properties of these defects have also been investigated by computational works[19,21–23], the agreement with the experimental data has supported the assignment of their emission bands. The nonbridging oxygen is well characterized by a PL around 1.9 eV with two excitation bands centered at 2.0 eV and 4.8 eV, however the PL position is influenced by the defect surrounding and a red shift down to $\sim$1 eV is observed when it interacts with oxygen vacancy defects, Si-Si[19]. The dioxasilyrane and the silanone emit overlapping PL bands in the visible range, around 2.2-2.4 eV, that can be resolved thanks to their different lifetimes[13]. On the other hand, O_2 oxygen molecule inside the silica NPs is characterized by a narrow IR emission centered at 0.97 eV excited in the near-IR range[24,25]. O_2 oxygen molecule has also been proposed for a fast (few ns) emission centered around 2.8 eV (blue band) that, after vacuum treatment, is enriched by vibronic lines above 3.0 eV (violet)[26]. The origin of the blue band has been associated with a defects pair consisting of a dioxasilyrane, $Si(O_2)$, and a silylene, Si••, its formation being induced by a dehydroxylation reaction of adjacent geminal Si-OH groups[27,28]. On the basis of this model, the UV light causes the photolysis of the dioxasilyrane making free O_2 in the excited state; the subsequent emission gives rise to the blue band coupled with the O_2 stretching phonon modes. This hypothesis is supported by the close similarity of the PL characteristics observed in nanocrystals of Al_2O_3 (γ-alumina), structurally and compositionally different from amorphous silica NPs. The understanding of the excitation/emission pathway giving rise to this structured PL is currently debated[26,29–31].

In this work we deal with the spectroscopic characterization of the visible PL associated with silica surface defects and the effects induced by vacuum treatments. We synthesized porous silica NPs by sol-gel technique and investigated their

[a] *Dipartimento di Fisica e Chimica, Università di Palermo, I-90123 Palermo, Italy; E-mail: marco.cannas@unipa.it*

structural and morphological properties. These systems are suitable to our purpose because of their very high specific surface that enhances the amount of luminescent defects. Our experimental approach is based on time-resolved luminescence spectroscopy combined with a tunable laser source that allows to discern between the vibronic lines and the blue band. The obtained results are useful to address the structural properties of these luminescent defects.

2 Experimental Methods

Silica NPs investigated in the present work were synthesized using a modified Stöber sol-gel route[32]. To obtain the colloidal solution, 70 mmol of TEOS (Aldrich, 99.99%) with 0.3 mol of water, 0.4 mol of ethanol (Sigma-Aldrich, absolute $\geq$ 99.5%) and with 1.5 mmol of ammonium hydroxide (Sigma-Aldrich, 29% NH_3 basis) were mixed. The solution was stirred in ultrasonic bath for 40 minutes and after two hours it was centrifuged for one hour at 8000 rpm, so as to favor the precipitation of silica NPs. The precipitate was separated by the supernatant to take away the unreacted species. Silica powders were washed twice with water for one hour at 8000 rpm and one more time with acetone in the same conditions. During the centrifuge cycles the temperature was maintained within the interval 23-28°. The precipitate was finally dried for one week in ambient atmosphere. The resulting material is a white granular powder.

Morphological details were provided by the Atomic Force Microscopy (AFM) investigation. The powder, as produced, was dispersed in ethanol and the solution was deposited on a mica substrate. After drying in vacuum, tapping mode amplitude modulated AFM measurements were acquired in air by a Multimode V (Veeco Instruments) equipped with a PointProbe Plus Silicon SPM (typical apical radius of 5-10 nm).

To identify the structure of the synthesized material, Fourier Transform (FT) -Raman and -IR spectra were acquired by a FT-Raman Spectrometer (Bruker RAMII), equipped with a 500 mW Nd:YAG laser (fundamental at 1064 nm), and a Bruker FT-IR spectrophotometer (VERTEX-70). The spectral resolution was 5 cm^{-1} and 1 cm^{-1} for Raman and IR absorption spectra, respectively.

The investigation of the emission properties was carried out by the time-resolved PL technique. Tunable excitation pulsed light (pulse width $\sim$5 ns, repetition rate 10 Hz) was provided by a VIBRANT OPOTEK optical parametric oscillator laser system, pumped by the third harmonic (3.50 eV) of a Nd:YAG laser and equipped with a second harmonic generation crystal. The pulse energy was monitored with a pyroelectric detector and the Fluence/pulse was maintained at Φ=0.2 mJ/cm^2, low enough to avoid the generation of luminescent defects[12]. The emitted light was spectrally resolved by a monochromator (SpectraPro 2300i, PI/Acton) equipped with two gratings: one, with 150 grooves/mm and blazed at 300 nm, has a spectral resolution of 20 nm/mm; the other, with 300 grooves/mm and blazed at 500 nm, has a resolution of 10 nm/mm. The spectra were acquired by an intensified charge coupled device (CCD) camera driven by a delay generator (PI-MAX Princeton Instruments) that sets the delay time from the laser pulse, T_D, and the integration time of the emitted light, ΔT. The experimental set-up allows us to control the atmospheric conditions thanks to a cryostat connected to a vacuum pump that stabilizes the pressure down to 10^{-6}mbar in about four hours. PL measurements were performed placing the sample in the cryostat in a standard front scattering geometry both in air and in vacuum. All the emission spectra reported in this work are corrected for the monochromator dispersion.

For the sake of clarity, we specify that FT-Raman, FT-IR and PL measurements were performed on self-supporting samples obtained pressing the powders, as-produced, at 300 MPa. In accordance with previous work, such a pressure is low enough to avoid structural changes of the material[33,34]. This procedure is needed in order to increase the signal-to-noise ratio. Only for the FT-IR investigation, the sample consists of a mixture obtained dispersing the synthesized powders in KBr (1% dilution). Moreover, the samples were heated in air at 300°C for two hours to enhance the characteristic emission in the visible spectral range and to remove any spurious contribution due to hydrocarbon contaminations[28,35,36].

3 Results

3.1 Structural and morphological characterization

Figure 1 shows the Raman spectrum of the as synthesized material and evidences the main typical features of nanostructured silica[37–39]. We mark the frequencies of the characteristic peaks: ν=410 cm^{-1} is the bending mode of oxygen in n-membered rings (n>4) and it is usually known as R line; ν=490 cm^{-1} is the breathing mode of 4-membered rings, usually called D_1 line; ν=800 cm^{-1} is the SiO_2 network optical mode; ν=980 cm^{-1} is the vibration of (OH)-group with respect to Si. We note that the Raman spectrum does not present the peak at ν=605 cm^{-1}, corresponding to the frequency of the 3-membered rings breathing mode (D_2 line), its absence is generally attributed to the porosity of silica[40,41]. In contrast with previous studies[24], we do not observe any signal around 1540 cm^{-1}: this shift from the Nd:YAG laser excitation corresponds, in fact, to an absolute energy of 0.97 eV identifying the IR emission of singlet O_2 in silica[42].

Further information on the structural properties of the material are given by the IR spectrum reported in Figure 2, where several wide bands are observed. The frequencies associated with the vibration modes in the silica structure are identified on the basis of experimental and simulation works[38,43]:

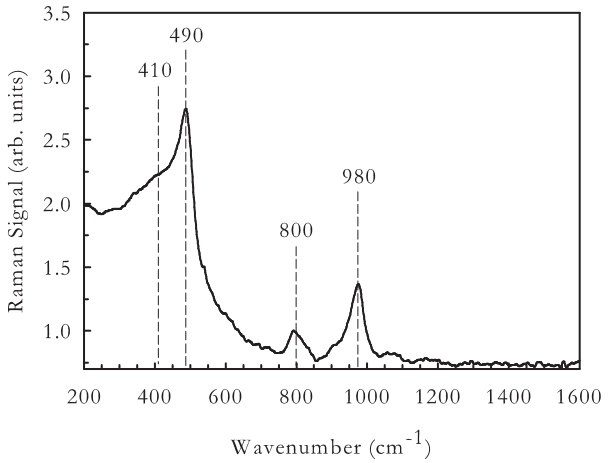

Fig. 1 Raman spectrum of the synthesized material. Dashed lines indicate the position of the characteristic Raman active structures of silica nanoparticles in cm^{-1}.

ν=459 cm^{-1} is the bending; ν=800 cm^{-1} is the symmetric stretching; ν=1095 cm^{-1} and ν=1200 cm^{-1} are the transversal and longitudinal asymmetric stretching, respectively. The OH related bands are also found: ν=980 cm^{-1} is the (OH)-Si stretching mode; the broad band around ν=3400 cm^{-1} originates from the overlap of different O-H stretching modes (adsorbed water, isolated, terminal and geminal silanols)[44].

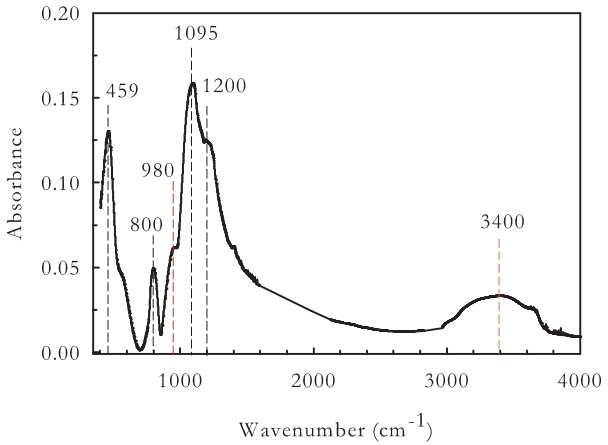

Fig. 2 IR spectrum of the synthesized silica NPs. Dashed lines indicate the position in cm^{-1} of the characteristic IR active structures related to the silica network (black) and to OH group (red).

The AFM image reported in Figure 3 shows isolated silica nanoparticles with size of about 10 nm.

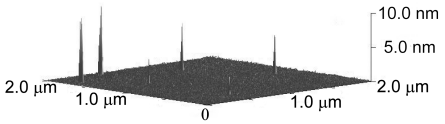

Fig. 3 AFM image of isolated nanoparticles composing the synthesized material.

3.2 Photoluminescence properties

Figure 4 summarizes the time resolved luminescence properties of the sample in air. In the panel (A) the PL spectrum is reported: it is acquired exciting at E_{exc}=4.96 eV, with T_D=10 ns and ΔT=100 ns. It consists of a broad band centered at 2.80±0.02 eV, with a full width at half maximum (FWHM) of 0.80±0.03 eV. Monitoring the peak intensity on varying E_{exc}, we obtained the blue band PL excitation (PLE) profile reported in Figure 4(B). It evidences two excitation maxima: one around E_{exc}=3.3 eV, the other, less intense, around E_{exc}=5.3 eV. The decay kinetics of the blue band is reported in Figure 4(C). The curve is obtained monitoring the peak intensity of the PL spectrum excited at E_{exc}=4.96 eV and integrated for ΔT=1ns on varying the delay time after the laser pulse is extinguished, from T_D=5 ns to T_D=31 ns. For the sake of clarity, in the same graph the decay of the laser pulse is also reported. The non-linear trend in the semilogarithmic plot evidences that the blue band decay deviates from a pure exponential. This behavior is typical of disordered systems with luminescent defects having distributed decay rates[36]. To account for such a decay rate, a best fit procedure was carried out using the stretched exponential function $I(t) = I_0 exp[-(t/\tau)^{\gamma}]$, where the lifetime τ is the time necessary to reduce the PL intensity by a factor e and the stretching parameter γ measures the deviation from a pure exponential[45]; we get τ=4.86±0.03 ns and γ=0.84±0.02.

We studied the blue PL also in vacuum environment using the same acquisition parameters applied for air detection (E_{exc}=4.96 eV, T_D=16 ns and ΔT=100 ns). Immediately after purging air, we noted the appearance of a structured emission between 3.0 and 3.5 eV. Over the time, on decreasing the pressure in the cryostat up to $\sim 10^{-6}$mbar, after 24 hours, the overall PL intensity increases and the structured PL sharpens. Figure 5 shows the comparison between the spectrum emitted from the sample in air and that stored in vacuum for 24 hours.

The structured PL can be isolated by opportunely setting the excitation laser energy and the time detection parameters. Its spectroscopic properties are reported in Figure 6: emission and excitation patterns are shown in the panel (A) whereas the PL decay is reported in the panel (B). The PL spectrum in (A) is obtained exciting the sample at E_{exc}=3.69 eV, setting ΔT=250 ns and delaying the acquisition from the

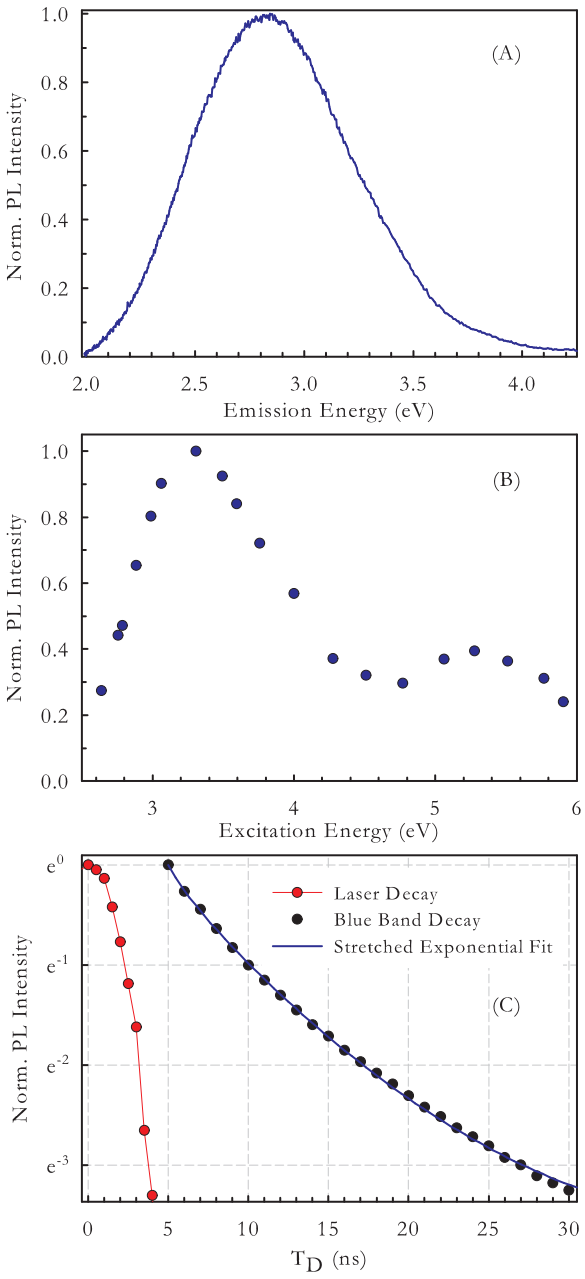

Fig. 4 (A) Emission spectrum of the synthesized sample acquired in air under E_{exc}=4.96 eV with T_D=10 ns and ΔT=100 ns. (B) Excitation energy dependence monitored at the maximum PL amplitude. (C) Semilogarithmic plot of the PL decay monitored at E_{em}= 2.8 eV under excitation E_{exc}= 4.96 eV (black dots) and of the laser pulse at 4.96 eV (red dotted line); the full blue line is the best fit stretched exponential curve.

laser pulse by T_D=115 ns, so as to remove from the spectrum

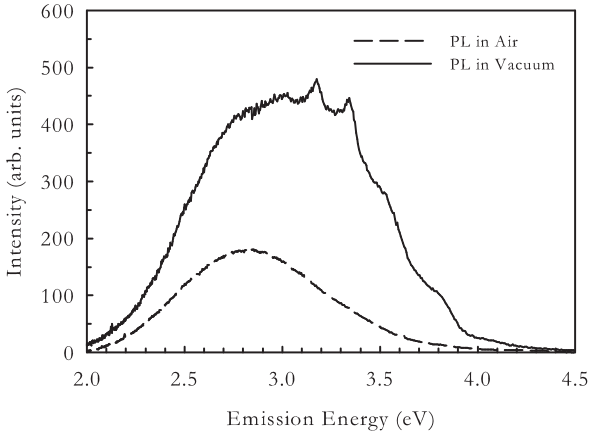

Fig. 5 PL spectrum emitted by the synthesized sample stored in air (dashed line) and in vacuum for 24 hours (continous line). Both spectra are excited at E_{exc}=4.96 eV, acquired with T_D=16 ns and ΔT=100 ns.

the blue band contribution decaying in few ns (see panel (C) of Figure4). A vibronic progression with four peaks spaced ΔE∼0.17 eV (∼1370 cm^{-1}) is evident, the position of the peaks being: 3.340±0.005 eV, 3.170±0.005 eV, 3.00±0.02 eV, 2.83±0.02 eV. Moreover, other PL peaks are observed at 3.290±0.005 eV and 3.245±0.005 eV. The PLE profile was obtained acquiring PL spectra at different excitation energies. As evidenced in the panel (A), the PLE pattern monitored at E_{em}=3.340 eV is also structured and shows two peaks centered at 3.69±0.01 eV and 3.85±0.02 eV. The PL decay shown in the panel (B) is monitored at E_{em}=3.34 eV, starting from T_D=30 ns to avoid the overlap with the blue PL: by a best fit procedure with a stretched exponential law we determine the lifetime τ=90±2 ns and the stretching parameter γ=0.70±0.02.

4 Discussion

The above reported results, based on AFM, FT-Raman and -IR spectroscopy, have proved the effectiveness of the sol-gel production of porous silica NPs with diameter of about 10 nm and decorated with OH groups. The time-resolved PL technique allowed us to distinguish two contributions in the UV-visible emission already observed in other nano-sized silica systems but not clearly disentangled up to now. One is the typical blue PL band centered at 2.8 eV, with a FWHM∼0.8 eV, observed both in air and in vacuum. This emission is characterized by a stretched exponential decay (τ≈5 ns and γ≈0.84) and a PLE spectrum with two bands centered around 3.3 eV and 5.3 eV. These features are in good accordance with

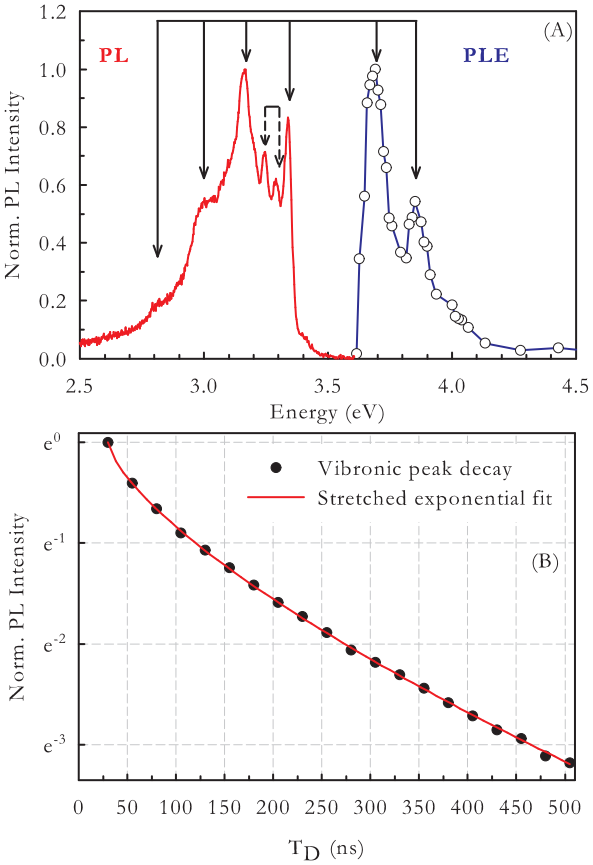

Fig. 6 (A) Emission and excitation features of the vibronic structures in vacuum: the PL spectrum (red line) is excited at E_{exc}=3.69 eV and acquired with T_D=115 ns and ΔT=250 ns. The PLE spectrum (circles)is obtained monitoring the excitation energy dependence of the peak at 3.34 eV, the blue line acts as a guide for viewing purpose. Solid arrows identify the vibronic progression spaced 0.17 eV (1370 cm^{-1}); dashed arrows point the progression spaced 0.045 eV (360 cm^{-1}). (B) Semilogarithmic plot of the PL decay monitored at E_{em}= 3.34 eV from T_D=30 ns to T_D=505 ns under excitation E_{exc}= 3.69 eV (black dots); each spectrum is integrated for ΔT=25 ns. The full red line is the best fit stretched exponential curve.

works dealing with the emission properties of nanosized silica or silica with nanosized pores[10,27,28,36,46]. The second contribution is a vibronic structured PL in the 3.0-3.5 eV violet range, characterized by a stretched exponential decay ($\tau \approx 90$ ns and $\gamma \approx 0.70$) and a PLE spectrum with two sharp peaks at 3.69 eV and 3.85 eV. Only on the basis of spectroscopic considerations, the comparison between the emission, excitation and decay properties clearly proves that the violet vibronic progression and the blue band have to be originated by two distinct defects, in contrast with previous suggestions[26].

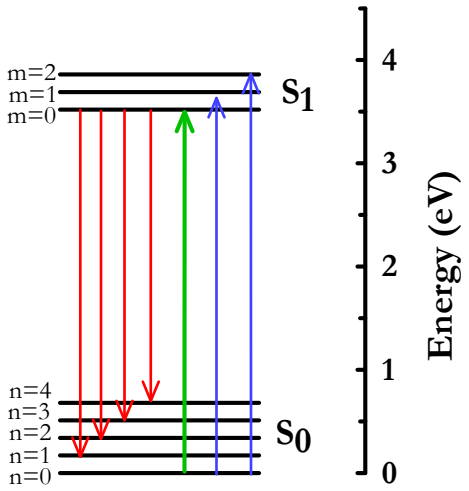

Fig. 7 Energy levels scheme associated to the structured PL/PLE pattern. The red and blue arrows refer to the emission and excitation transitions, respectively; the green arrow highlights the ZPL.

Since this structured PL is peculiar to vacuum environment, we can hypothesize that it originates from a defect located at the surface: in air the PL is quenched by the interaction of the luminescent defect with molecular species of the ambient atmosphere, such as molecular oxygen and nitrogen; the vacuum treatment removes these species, thus activating the optical emission. The observation of a well defined vibronic pattern proves that this luminescence originates from molecular species in SiO_2 NPs with electron-phonon coupled vibrational motion. The excitation/emission pattern evidences a common vibronic progression with peaks spaced by ΔE∼0.17 eV, in agreement with a mirror-like symmetry. This finding identifies a hard vibrational mode ($\nu_H \sim 1370$ cm^{-1}) much larger than the thermal energy at room temperature $k_BT \sim 0.025$ eV (∼200 cm^{-1}). This mode is linearly coupled with the excitation and emission electronic transitions. It is worth noting that the Stokes shift of ∼0.35 eV, measured by the difference between the excitation peak at 3.69 eV and the emission at 3.34 eV, is nearly $2 \times h\nu_H$; this allows us to roughly estimate the Huang-Rhys factor, S∼1, that is consistent with a low electron-phonon coupling. Then, we can locate the zero phonon line (ZPL) around 3.52 eV and consequently attribute the observed peaks to allowed transitions, in accordance with the fast decay time (∼100 ns), between the vibrational levels of two singlet electronic states. Such transitions are graphically represented in the energy levels scheme reported in Figure 7: the excitations at 3.69 eV and 3.85 eV correspond to the absorption from the lower vibrational level (n=0) of the electronic ground state S_0 towards the vibrational levels m=1 and m=2 of the electronic excited state S_1; the emission peaks at 3.34 eV, 3.17 eV, 3.00 eV and 2.83 eV correspond to the

radiative decay from the lower vibrational level (m=0) of S_1 down to the vibrational levels n=1, n=2, n=3 and n=4 of S_0. The additional peaks spaced by 0.045 eV, observed in the PL spectrum, indicate that this electronic transition is also coupled with a soft vibrational mode of frequency $\nu_S \sim 360$ cm^{-1}. It is worth noting that both the vibrations are not observed either in the Raman or in the IR absorption spectra. In contrast, the PL spectroscopy offers much more selectivity in detecting the vibrations coupled to the electronic transitions of defects.

The comparison with literature data allows us to discuss the origin of the structured PL centered in the range 3.0-3.5 eV. A vibronic progression with lines spaced by $\nu_H \sim 1370$ cm^{-1} has been observed both in silica based organic-inorganic hybrid[47] and in evacuated silica nanoparticles[26]. In contrast, the progression with lines spaced by $\nu_S \sim 360$ cm^{-1} has not been resolved in previous works, at least to our knowledge. Therefore the assignment of the combined ν_H and ν_S vibronic lines to a specific group at silica surface is not experimentally supported yet[14,48]. We rule out Si-H and the Si-OH in view of their different PL properties[15,16]. Alternatively, computational works dealing with the optical properties of defects peculiar to surface silica have pointed out vibration modes with frequencies in good agreement with that observed in our PL spectra. In particular, Mebel et al.[48] have predicted the superposition of two vibrational progressions around 1300 cm^{-1} and 360 cm^{-1} in the PL spectra of silanone. In accordance with that model, the excitation of this defect leads to an elongation of the Si=O double bond, accompanied by its out-of-plane distortion respect to the basal O[23,48]; the frequencies 1300 cm^{-1} and 360 cm^{-1} are associated with the Si=O stretching and bending, respectively. On the other hand, the dioxasilyrane ring Si(O_2) is characterized by four vibrations bands with frequencies in the range $\sim$800-1200 cm^{-1} [21]. However, the role of silanone or dioxasilyrane as defects candidate for the origin of the observed vibrations coupled to violet PL spectrum is weakened by some findings. Both defects emits a green PL[13,21,23], moreover the silanone is not stable in ambient atmosphere because of the reaction with water molecules[13].

In a recent work[26] the structured PL with lines spaced $\sim$1350 cm^{-1} has been assigned on the basis of the similarities between silica and γ-alumina nanoparticles. In agreement with the defects pair model[27], Si(O_2) and Si$\bullet\bullet$, proposed to explain the origin of the blue band, the vibronic progression has been associated with the O_2 Herzberg III decay transition from $A'^3\Delta_u$ to $X^3\Sigma_g^-$ electronic states[49], where O_2 in its excited state originates by the transient photolysis of the dioxasilyrane. To this regard, our data allow us to make the following considerations: first of all, for the free O_2 the ZPL of the $A'^3\Delta_u$ to $X^3\Sigma_g^-$ transition is 34387 cm^{-1} (4.26 eV) and the stretching frequency for the $X^3\Sigma_g^-$ ground state is 1580 cm^{-1} [50,51]; these values are significantly larger than those measured in our experiment: ZPL$\approx$3.52 eV, $\nu_H \sim 1370$ cm^{-1}. Moreover, the observation of the additional vibronic peaks spaced 360 cm^{-1} is not consistent with a diatomic molecule. On the other hand, whatever the defect responsible for the blue band, the spectroscopic data exclude the possibility that a single defect gives rise to both the blue band and the vibronic progression.

5 Conclusions

The modified St*ö*ber sol-gel route that we used to synthesize silica nanoparticles is successful to produce a porous material exhibiting a PL in the UV-visible range. Vacuum treatment leads to the appearance of a structured emission in the violet range coupled with two vibration modes: a hard one ($\nu_H \sim 1370$ cm^{-1}) with a low Huang-Rhys factor (S$\sim$1) and a soft one ($\nu_S \sim 360$ cm^{-1}). On the basis of the excitation and decay properties, we propose that the violet structured luminescence has a different origin than the blue band which, in the current literature, is associated with a defects pair consisting of a dioxasilyrane and a silylene. The observation of two vibration modes is consistent with a defect structure containing more than two atoms, the measured frequencies at 1370 cm^{-1} and 360 cm^{-1} being in agreement with the stretching and bending vibrations calculated for O_2 related defects.

6 Acknowledgements

The work was partially supported by FAE project, PO FESR Sicilia 2007/2013 4.1.1.1. and FFR 2012/2013 of University of Palermo. We express our gratitude to Prof. R. Boscaino, Dr. F. Messina and the group of the Laboratory of Advanced Materials Physics (Palermo University)(http://www.fisica.unipa.it//amorphous) for the valuable and stimulating discussions. G.Napoli and G.Tricomi are acknowledged for their technical assistance.

References

1 J. M. Rosenholm, C. Sahlgren and M. Lindn, *Nanoscale*, 2010, **2**, 1870.
2 K. Ma, U. Werner-Zwanziger, J. Zwanziger and U. Wiesner, *Chem. Mater.*, 2013, **25**, 677.
3 H. Chen, Z. Zhen, W. Tang, T. Todd, Y. Chuang, L. Wang, Z. Pan and J. Xie, *Theranostics*, 2013, **3**, 650.
4 A. Zatsepin and E. Buntov, *J. Non Cryst. Solids*, 2009, **355**, 1123.
5 I. J. Kramer and E. H. Sargent, *Chem. Rev.*, 2014, **114**, 863.
6 W. G. J. H. M. van Sark, J. de Wild, J. K. Rath, A. Meijerink and R. E. Schropp, *Nanoscale Res. Lett.*, 2013, **8**, 1.
7 S. Banerjee and A. Datta, *Langmuir*, 2009, **26**, 1172.
8 S. Bonacchi, D. Genovese, R. Juris, M. Montalti, L. Prodi, E. Rampazzo and N. Zaccheroni, *Angew. Chem. Int. Ed.*, 2011, **50**, 4056.
9 C. D. S. Brites, V. T. Freitas, R. A. S. Ferreira, A. Mill*á*n, F. Palacio and L. D. Carlos, *Langmuir*, 2012, **28**, 8190.
10 G. L. Davies, J. McCarthy, A. Rakovich and Y. K. Gun'ko, *J. Mater. Chem.*, 2012, **22**, 7358.
11 H. Jaganathan and B. Godin, *Adv. Drug Del. Rev.*, 2012, **64**, 1800.

12 L. Spallino, L. Vaccaro, S. Agnello and M. Cannas, *J. Lumin.*, 2013, **138**, 39.
13 L. Vaccaro, A. Morana, V. Radzig and M. Cannas, *J. Phys. Chem. C*, 2011, **115**, 19476.
14 A. Rimola, D. Costa, M. Sodupe, J. Lambert and P. Ugliengo, *Chem. Rev.*, 2013, **113**, 4216.
15 Y. D. Glinka, S. H. Lin and Y. T. Chen, *Appl. Phys. Lett.*, 1999, **75**, 778.
16 C. Carbonaro, F. Clemente, R. Corpino, P. Ricci and A. Anedda, *J. Phys. Chem. B*, 2005, **109**, 14441.
17 G. Renger and B. Hanssum, *Photosynth. Res.*, 2009, **102**, 487.
18 G. Iovino, S. Agnello, F. M. Gelardi and R. Boscaino, *J. Phys. Chem. C*, 2012, **116**, 11351.
19 A. S. Zyubin, Y. D. Glinka, A. M. Mebel, S. H. Lin, L. P. Hwang and Y. T. Chen, *J. Chem. Phys.*, 2002, **116**, 281.
20 V. N. Bagratashvili, S. I. Tsypina, V. A. Radtsig, A. O. Rybaltovskii, P. V. Chernov, S. S. Alimpiev and Y. O. Simanovskii, *J. Non Cryst. Solids*, 1995, **180**, 221.
21 K. Raghavachari and G. Pacchioni, *J. Chem. Phys.*, 2001, **114**, 4657.
22 K. Raghavachari, D. Ricci and G. Pacchioni, *J. Chem. Phys.*, 2002, **116**, 825.
23 M. A. Zwijnenburg, A. A. Sokol, C. Sousa and S. T. Bromley, *J. Chem. Phys.*, 2009, **131**, 034705.
24 S. Agnello, M. Cannas, L. Vaccaro, G. Vaccaro, F. M. Gelardi, M. Leone, V. Militello and R. Boscaino, *J. Phys. Chem. C*, 2011, **115**, 12831.
25 S. Agnello, L. Vaccaro, M. Cannas and K. Kajihara, *J. Non Cryst. Solids*, 2013, **379**, 220.
26 A. Anjiki and T. Uchino, *J. Phys. Chem. C*, 2012, **116**, 15747.
27 T. Uchino, N. Kurumoto and N. Sagawa, *Phys. Rev. B*, 2006, **73**, 233203.
28 A. Aboshi, N. Kurumoto, T. Yamada and T. Uchino, *J. Phys. Chem. C*, 2007, **111**, 8483.
29 A. Nishimura, S. Harada and T. Uchino, *J. Phys. Chem. C*, 2010, **114**, 8568.
30 C. M. Carbonaro, R. Corpino, P. C. Ricci, M. Salis and A. Anedda, *J. Mater. Sci.*, 2013, **48**, 4452.
31 C. M. Carbonaro, R. Corpino, P. Ricci and D. Chiriu, *J. Non Cryst. Solids*, 2014.
32 T. Stȍber and A. Fink, *J. Colloid Interface Sci.*, 1968, **26**, 62.
33 J. Wu, X. Liu and S. H. Tolbert, *J. Phys. Chem. B*, 2000, **104**, 11837.
34 M. Mandal and K. Landskron, *Acc. Chem. Res.*, 2013, **46**, 2536.
35 L. L. Hench and J. K. West, *Chem. Rev.*, 1990, **90**, 33.
36 L. Vaccaro, G. Vaccaro, S. Agnello, G. Buscarino and M. Cannas, *Solid State Commun.*, 2010, **150**, 2278.
37 T. Yamada, M. Nakajima, T. Suemoto and T. Uchino, *J. Phys. Chem. C*, 2007, **111**, 12973.
38 M. Corno, A. Pedone, R. Dovesi and P. Ugliengo, *Chem. Mater.*, 2008, **20**, 5610.
39 G. Vaccaro, S. Agnello, G. Buscarino and F. M. Gelardi, *J. Phys. Chem. C*, 2010, **114**, 13991.
40 C. J. Brinker and G. W. Scherer, *SOL-GEL SCIENCE, The Physics and Chemistry of Sol-Gel Processing*, Academic Press, Inc., San Diego, 1990.
41 C. Kinowski, M. Bouazaoui, R. Bechara, L. L. Hench, J. M. Nedelec and S. Turrell, *J. Non Cryst. Solids*, 2001, **291**, 143.
42 L. Skuja and B. Güttler, *Phys. Rev. Lett.*, 1996, **77**, 2093.
43 C. T. Kirk, *Phys. Rev. B*, 1988, **38**, 1255.
44 P. Innocenzi, *J. Non Cryst. Solids*, 2003, **316**, 309.
45 D. C. Johnston, *Phys. Rev. B*, 2006, **74**, 184430.
46 C. Carbonaro, P. Ricci, R. Corpino, M. Marceddu and A. Anedda, *J. Non Cryst. Solids*, 2011, **357**, 1904.
47 A. Nishimura, N. Sagawa and T. Uchino, *J. Phys. Chem. C*, 2009, **113**, 4260.
48 A. Mebel, A. Zyubin, M. Hayashi and S. Lin, *Thin Films and Nanostructures*, 2007, **34**, 67.
49 G. Herzberg, *Can. J. Phys.*, 1953, **31**, 657.
50 T. G. Slanger and R. A. Copeland, *Chem. Rev.*, 2003, **103**, 4731.
51 P. H. Krupenie, *J. Phys. Chem. Ref. Data*, 1972, **1**, 423.

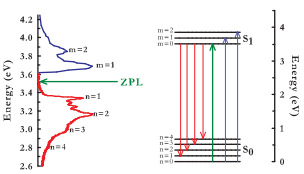

Vibrational pattern coupled to excitation and emission transitions of surface defects in silica nanoparticles in vacuum